J. Inst. Eng. India Ser. D
https://doi.org/10.1007/s40033-024-00698-5

ORIGINAL CONTRIBUTION

Analysis of Lightweight Braking Material System for an ATV

Mohan Poojari[1] · **Harshitha Madhusoodan Jathanna**[2] · **V. S. Vijay**[3] · **Sharun Mendonca**[3] · **Rolvin DSilva**[3]

Received: 3 January 2024 / Accepted: 15 March 2024

Abstract An all-terrain vehicle (ATV) was designed and manufactured to participate in the SAE Baja, India event, and in the present work, we have considered one subsystem, namely the braking system. The design of lightweight components helps optimize a system overall for greater effectiveness and efficiency. It may then result in a decrease in the carbon footprint. The goal of the study was to explore the performance of a lightweight brake system for ATV applications using numerical methods. An optimized brake system for ATV car use was the focus of the study. Structural steels, i.e. SS410 and SS420, along with aluminium alloys were the materials used. The suggested ATV brake system was examined using the finite element method (FEM). With a value of 297 MPa, the most optimized design showed the maximum stress. The most optimized brake lever, according to the stress–strain graph, has the greatest stress and highest strain value. However, aluminium alloy may be used to create the lightest component.

Keywords All-terrain vehicle · Lightweight material · SS410 and SS420 · Brake system · Brake callipers

✉ Mohan Poojari
mohanshiruru@gmail.com

[1] NITTE (Deemed to be University), Department of Mechanical Engineering, NMAM Institute of Technology, Nitte, Karnataka 574110, India

[2] NITTE (Deemed to be University), Department of Biotechnology Engineering, NMAM Institute of Technology, Nitte, Karnataka 574110, India

[3] Department of Mechanical Engineering, St Joseph Engineering College, Mangaluru, Karnataka 575028, India

Introduction

The braking system deals with the deceleration of the vehicle by the means of transfer of pressure applied by pressing the brake pedal via brake lines which have hydraulic fluids in them. A successful braking system ensures all wheels lock at the same moment and stop the vehicle within the acceptable distance and time. The cars designed in the previous year for SAE BAJA event had achieved a braking distance of 2 m. Given the lighter weight of the vehicle and the fact that the braking was designed specifically keeping in mind the dynamic abilities of the car, it can improve upon the stopping distance greatly [1–4]. Disc brakes were preferred over drum type because of factors such as the high possibility of mud and debris gathering in the space between the shoe and the drum in drum brakes. The disc brake is less bulky and weighs less compared to the drum type. Efficient cooling or better heat dissipation and more resistance to water are key features of the disc brakes. Also, disc brakes have more stopping power than drum brakes which greatly simplify the design of the wheel assembly and reduce its weight. As the ATV application is mainly off-roading, for this reason anti-lock braking system (ABS) was not considered in the design.

Materials

When the brake is applied, the calliper, which is a component of a disc brake, presses the brake pads on the rotor on both sides. Each brake calliper receives hydraulic pressure from the master cylinder when the driver's foot presses the brake pedal [5]. To apply the brake, one or more pistons are forced outward by fluid pressure inside the calliper. The hydraulic pressure decreases and the callipers lose their hold when the brake pedal is removed. While pressure is

Published online: 23 April 2024

removed, the square-cut seals around the calliper pistons would want to revert to their former shape since they are deformed while the pistons move [6]. This aids in the pistons' small retractions, enabling the pads to retract from the rotors. Drum brakes require return springs, which are not needed in this situation. A wide variety of calliper models were investigated such as Bybre, Royal Enfield, WilWood, etc. After comparing their functioning, it was concluded that a dual-piston calliper with a piston on each side and side-mounted bleeding screws were optimum. WilWood and Vespa KBX were the choices available, but the WilWood callipers cost three times as much as Vespa. For this reason, the Vespa Calliper was selected. The Vespa KBX callipers have a pad width of 32 mm, a base length of 35 mm, and a total thickness of 7.5 mm. They have a weight of 500 g. Four of these have to be used, and suitable guidelines were given to the suspension team by the brakes team for designing the mounts on the wheel assembly further to build a stable and well-performing ATV.

A control mechanism called a master cylinder (MC) transforms non-hydraulic pressure typically generated by the driver's foot into hydraulic pressure. The operation follows Pascal's law, which states that force applied to the greater input area of a cylinder results in the exit of the cylinder being filled with a high-pressure fluid. There are two distinct hydraulic chambers in the tandem master cylinder [7–9]. In essence, this separates the hydraulic brake circuits into two. The car can still be stopped by using the other circuit if one of these stops working. While using a single brake circuit, the stopping distance was greatly enhanced. Among the car's most crucial safety features is this one. When the brake pedal is depressed under normal circumstances, the brake fluid will transfer pressure to the front and rear brakes. For this purpose, an investigation of a wide range of MC models was done, and based on previous experience of building ATVs, BOSCH tandem MC was selected as they are simple in construction and highly reliable, and more importantly, they are cheaper than most other options while functioning similarly.

There are two types of brake layouts, namely H split and X split. In H split brake, the front brake assembly was connected to one outlet of the master cylinder and the rear brake assembly to another outlet of the master cylinder. In the case of an X split brake, one front and one rear calliper are connected to one part of the brake master cylinder and the remaining two are connected to the other outlet of the master cylinder. If a master cylinder segment fails, the X split brake arrangement guarantees that at least either of the rear wheels remains under control (power wheels). This makes braking better and reduces the effect of the failure of the master cylinder. For this purpose, X split configuration was chosen [10]. The organization of the braking system and the pedal box was designed after performing multiple iterations. Research on all the components was done and the OEM components were chosen and ordered while plans for the design and fabrication of the custom components were made. Choosing the best brake calliper and master cylinder models, brake calculations were done and the braking parameters were determined accordingly [11–14]. The design for the brake disc was done, and the design was analysed to determine its factor of safety (FOS) and thermal characteristics. The material for the brake disc was chosen, and fabrication was done using laser cutting. After all, seven brake discs were fabricated, and they have been mounted to the wheel assembly [15–17]. The design for the pedal box was done and analysed after choosing the appropriate material. It was then fabricated by laser cutting and welding processes. Once all components were acquired, the brake lines were assembled and connected to the callipers and the master cylinder. The pressure switch was connected to the brake splitter and brake light connections were done. The pedal box was welded to the chassis, and the brake bleeding process was done to circulate the brake fluid to the entire brake circuit. The braking performance was tested and tuned to get the best possible stopping distance (Fig. 1).

The main function of the brake rotor is to retard the motion of the wheel. Previously, the team had used OEM brake discs from a bike TVS Apache RTR 150. However, these discs were large and weighed 400 g each which meant the wheel assembly needed to be bigger and use of bigger wheel was necessary [18–20]. To overcome this, it was decided to design a custom break disc according to the dimension of the wheel, breaking torque needed and heat dissipation characteristics while having the goal of reducing weight. The factors that must be determined are the effective area of pads, the minimum thickness of brake disc for the OEM calliper, the maximum temperature of the material, steady-state thermal analysis (temperature in one stop), static structural analysis, and so on.

A simpler approach was followed to select the material for the brake disc and it was looked into the industry standards and relied on literature. It is a well-known fact that when hardened, stainless steel resists corrosion more effectively. Therefore, it is an excellent option when resistance to a moderately corrosive environment is required for the final application and good formability and high strength are required. There are different materials suitable for the fabrication of disc brakes. However, the choice was between SS410 and SS420; considering the all-terrain application of the vehicle and from looking into the properties, SS410 was chosen over SS420 due to the following reasons. SS410 has a lower hardness than SS420 in the heat-treated condition, but the hardness obtained in SS 410 was adequate for disc brake application in motorcycles. SS410 has a better combination of hardness and toughness [15, 21–23]. The corrosion resistance of SS410 was marginally better. The heat treatment process for SS410 was simpler than that for

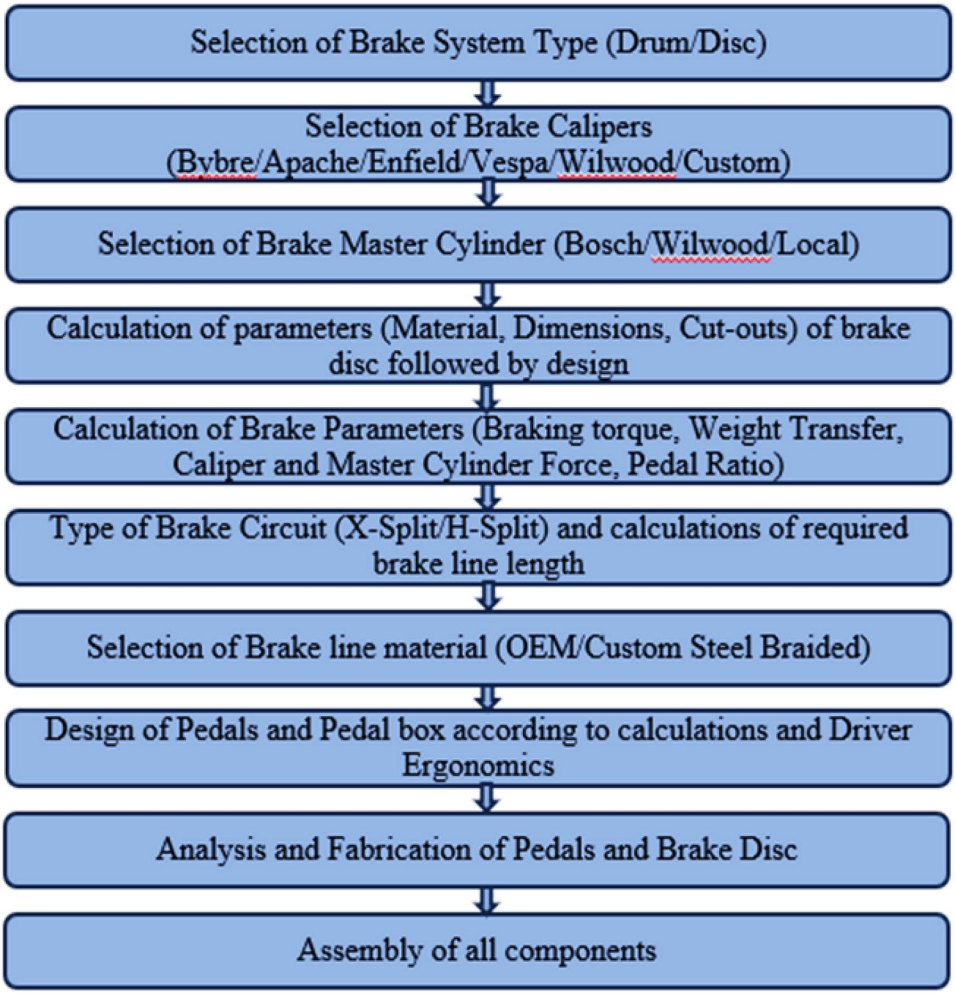

Fig. 1 Braking system flow-chart

SS420. Through induction hardening and quenching of the brake pad contact area on the disc, the required combination of hardness and toughness can be achieved comfortably with SS410. Special grades of SS410 with the addition of small elements, such as nitrogen, are available with consistent mechanical and thermal properties. The disc was designed in CATIA using the values obtained from calculations and dimensions obtained from information from the steering and suspension team. The properties of the material SS410 and the disc parameters obtained from calculations [24] are mentioned in Table 1.

Calculating normal forces with weight transfer: First, the forces required for the disc analysis were produced by applying the equations of moments to calculate normal forces at steady-state (static or constant velocity). It also helped to determine the pedal ratio. After conducting multiple iterations, the final values used are tabulated in Table 2.

SS410 sheets of 4.2 mm thick were purchased, and machining of the disc was done using a Laser cutting process to obtain the high level of accuracy needed. The disc was screwed onto the wheel assembly at the mounting points and thread sealant was applied to arrest the motion of the screws. The calliper was then mounted to the wheel assembly and further adjustments were made to maintain the gap between the pads and the disc. From past experience, it was observed that rubber brake lines are fragile and with the kind of conditions the brakes need to operate in, they are not suitable for the given application. Hence, steel braided brake lines and copper four-way brake splitters have been used to divide the circuit wherever necessary to obtain the X split configuration. One output per brake splitter was kept for the pressure switch which was needed for the brake light function [25–32].

Since no deviation from the rule book was allowed, the rule book requires us to provide a brake light which indicates when the brake pedal was pressed. For this, the hydraulic pressure switches have been provided in the brake circuit [33]. To monitor a process and produce an output when a predetermined pressure was attained, a pressure switch was used. To do this, a pressure switch applies process pressure to a piston or diaphragm, creating a force comparable to that of a range spring that has been pre-compressed. To find out

Table 1 Properties of SS 410 and disc parameters

Properties of SS 410					
Yield strength 0.2% offset		Ultimate tensile strength		Elongation in 2 in	Hardness
Psi	(MPa)	Psi	(MPa)	%	(max.)
42,000	290	74,000	510	34	96 Rb
Disc parameters					
Disc outer diameter	175 mm				
Disc thickness	4.2 mm				
Material	SS 410				
Mounting bolt	CSK M8 20 mm Alan key				
Convective holes	2 sets of 14				
Distance of first hole set from centre	78 mm				
Distance of second hole set from centre	68 mm				
Convective hole diameter	6 mm				
Number of slots	8				
Outer radius of flower pattern	43.5 mm				

Table 2 Brake values

Parameter	Value	Brake circuit parameters	
Dynamic loads	Front: 1678.5 N Rear:1264.5 N (Values taken based on vehicle weight, driver weight, maximum speed of the ATV and as per the SAE Baja rule book requirements)	Configuration	Front-rear X split
Coefficient of friction between Tyre and road surface	0.65–1 (Value taken as per the SAE Baja rule book requirements)	Master cylinder (bore, mm * stroke, mm)	Dual tandem (19.05 * 18)
Brake torque required per wheel	Front: 185.507 Nm Rear: 138.766 Nm	Calliper cylinder (bore * no of cylinder)	$27mm^2$
Force required per calliper cylinder	Front: 1203.02N Rear: 899.909 N	Calliper pad	Effective radii:96.375 mm Area:$8775.9mm^2$ Friction coefficient:0.4
Pedal force	400N (max) (Value taken based on driver foot pressure, stopping distance, dynamic conditions of the ATV and as per the SAE Baja rule book requirements)	Brake fluid	Dot 3
Pedal ratio	6:1		
Pedal travel	127 mm (Value taken based on driver foot pressure, ergonomics of the sitting posture, dynamic conditions of the ATV and as per the SAE Baja rule book requirements)		

if there was fluid pressure, one uses a pressure switch. As the sensing element, most pressure switches employ a bellow or diaphragm. To sound an alarm or start a control action, this sensing element's movement was utilised to trigger one or more switch connections. In this case, the pressure switch was used as a switch in the brake light circuit 2 pressure switches connected in series has been used. The brake light used was a 12-V LED element, and hence, a 12-V battery has been mounted using specially designed mounts (Fig. 2).

The pedal box has a general layout with the brake and accelerator pedal and master cylinder setup placed in the most functional position for driver comfort. The basis for the driver's comfort was the ability of the driver to drive the ATV in an ergonomically comfortable position in off-road

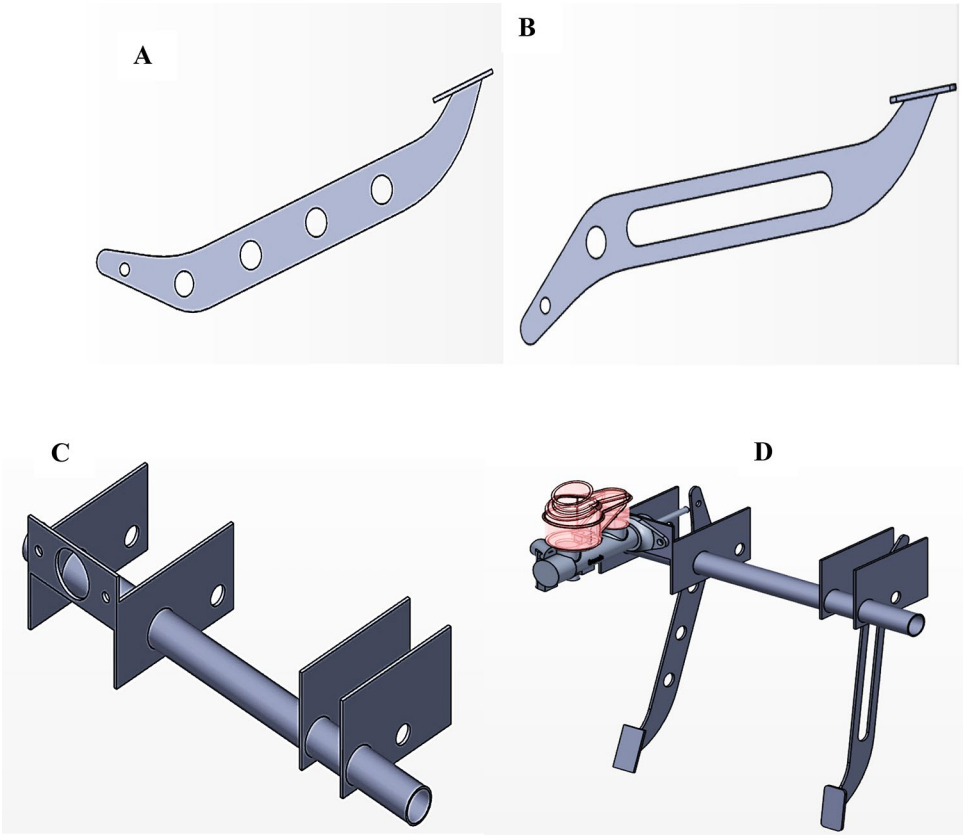

Fig. 2 Brake pedal design and assembly (A—design; B—accelerator pedal; C—mounting frame; D—pedal assembly)

conditions for continuous 5 h with smaller pit stops. Measurements of the driver had to be taken so that to determine the driver's reached for the complete actuation of the pedals. The pedal ratio for adding 150lbf to the master cylinders was taken into consideration while designing the brake pedal. It was also assumed that the actual force applied by the diver to the pedal was 400N. Hence, the pedal needs to withstand this load repeatedly; considering these considerations, the pedal was designed in CATIA [34–39]. The material chosen was 4130 sheet metal 3 mm thick as this material fits well considering the design parameters for the pedal to keep the weight as low as possible. To further reduce the weight, holes of different diameters were made in the pedal surface. Weight reduction of the ATV was of prime importance as it contributes to better manoeuvrability, increased performance, and lesser fuel consumption, which was the basic criterion of an ATV. The pedal ratio was 6:1, and to accommodate this M8 hole provides the flexibility of obtaining the required pedal ratio and it was cut into the pedal frame so that the pivot point can be provided there. Bushing of 16 mm diameter was also provided to accommodate the pivot and spring. A M6 hole was provided at the top to bolt the MC plunger [40–44].

The pedal was cut machined using laser cutting and the footrest will be welded to the frame. Bushing will also be machined and welded to the frame. The accelerator pedal will only need 50 N to actuate hence the design can be made lighter by cutting a slot into the frame. A M8 hole was provided for the pivot bolt and 16 mm diameter bushing was made around it. A M6 hole was made for the mounting of the throttle cable to be attached. The pedals, pivot bolts, master cylinders, stoppers, and line attachments must be mounted to a single chassis pipe which was welded to the chassis. For this, the appropriate side plates and holes were designed. After the individual components were manufactured, they were assembled and appropriate return springs and bolts were fixed [45–49]. The new pedal box produced was lighter and more reliable compared to the old vehicle. It was also comfortable and has proven its reliability over time.

Structural engineering challenges can be solved and quicker design decisions can be achieved with the help of ANSYS structural analysis software. Automation and customization of the solutions to the structural mechanics issues is possible with the finite element analysis (FEA) tools. Answers can be parameterized to analyse various design scenarios. For even more fidelity, a quick link to different physics analysis tools is possible. Throughout the business, engineers have been utilizing ANSYS structural analysis software to optimize their product designs and lower the cost of physical testing.

Results

ANSYS Workbench was used for the analysis of the disc.

Heat Flux = 27,000 W/m^2
Material = SS 410
Coefficient of convection [5] = 230 W/m^2 C
Clamping force = 3600 N
Braking torque: 230 Nm
Contact area = 8775.9 mm^2.

On the outside border of the resultant displacement fields, as seen in Fig. 3, the maximum value was obtained. It was in the radial direction that the plate tends to distort the most. Moreover, a greater distortion causing surface waviness was seen in the normal direction close to the inner circumference. It can move up to 0.244 mm in maximum. As seen in the image, the expansion grooves cause the plate to deform more tangentially. The material experiences plastic deformations because the stated thermo-mechanical load indicates the condition of the plate's excessive loading.

A combination of mechanical and thermal loads was considered. The requirement data served as the foundation for defining the loading conditions. Normal pressure was created by the pistons and was then transferred to the stator disc. The normal force Fn = 285 kN acting on the top surface of the rings expresses the load from the pistons. The typical direction of support was maintained for the bottom surface that was in contact with the stator. A friction force Ft = 64 kN operating in the circumferential direction was concentrated on the contact surface because there was friction between the stator and the ring. As the translational degrees of freedom in the tangential and radial directions were fixed, constraints have been set on the mounting slots. Figure 5 depicts boundary conditions [50–54].

The thermal load was factored in alongside the mechanical load. Heat was produced during braking between the stator and rotor discs and was sent to the plate via the rings' contact surfaces. Figure 4 displays the temperature fields that indicate the temperature load of the plates that were examined. The maximum temperature, 139 °C, was recorded on the friction surfaces, whereas the inner circle recorded the lowest temperature, around 80 °C. Both temperatures are well within the workability temperature limits of the selected material and with sufficient factor of safety. The structural FOS achieved was 3.22. There was an acceptable range for both values. High-strength stainless steel alloy, grade SS 410, was used to make the pressure plate [55–60]. This type of steel was stronger than traditional structural steels and has superior mechanical and corrosion resistance [61–65]. Table 1 provides information on its mechanical characteristics at room temperature (Figs. 5, 6).

A force of 400 N was applied on the footrest while constraining the pivot point for brake pedal analysis [66, 67].

Material of Pedal: AISI 4130
Tensile ultimate strength of material: 560 MPa
Tensile yield strength: 460 MPa
Factor of safety: 2.07
Maximum displacement: 1.2516 mm.

A force of 400 N was applied on the footrest while constraining the pivot point for accelerator pedal analysis [68–70] (Figs. 7, 8).

Material of Pedal: AISI 4130

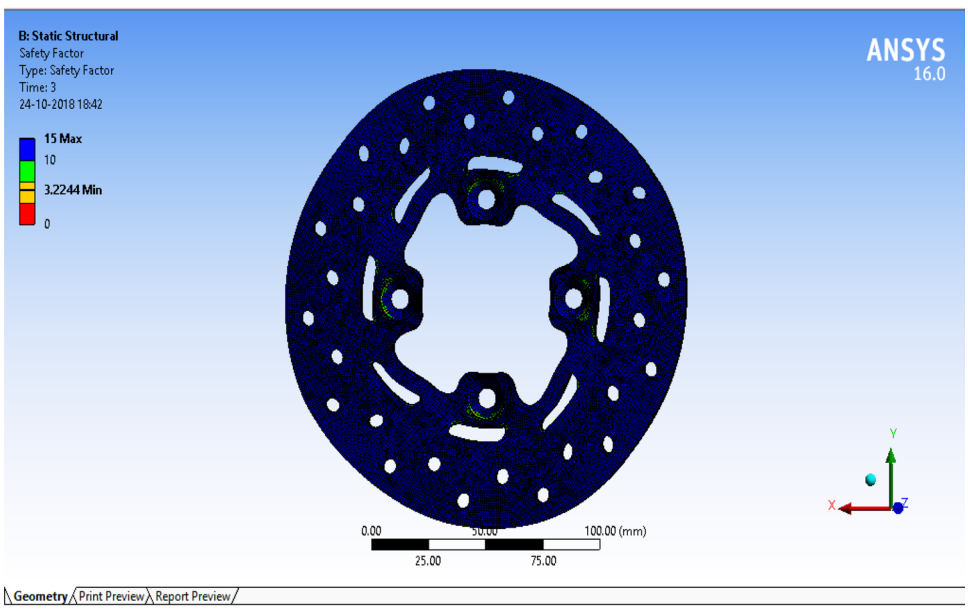

Fig. 3 Structural analysis of brake disc

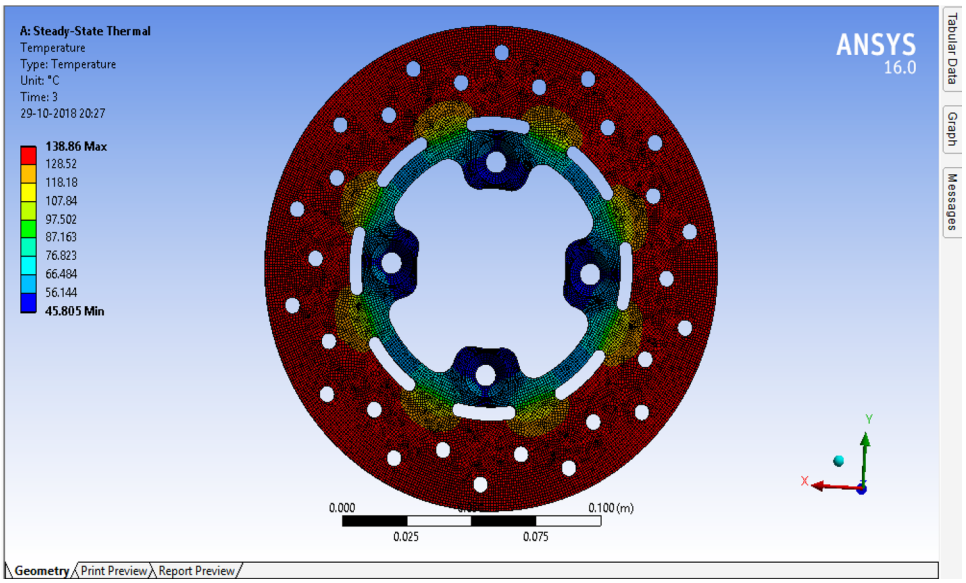

Fig. 4 Thermal analysis of brake disc

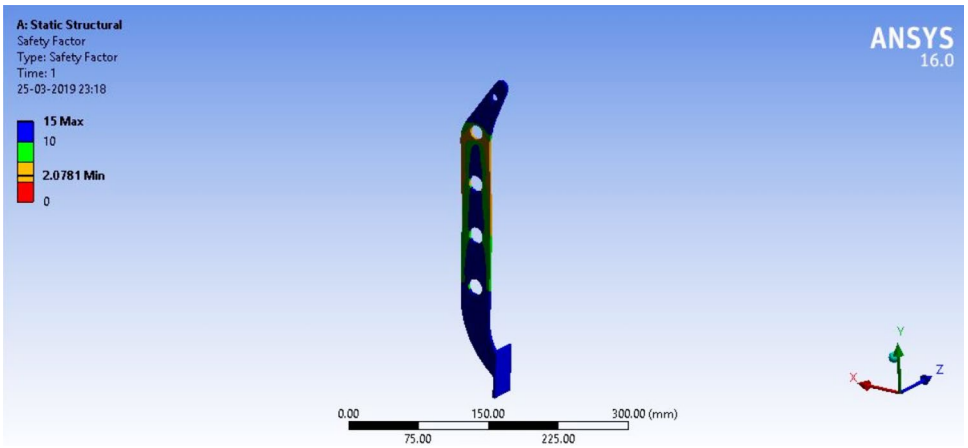

Fig. 5 FOS analysis of brake pedal

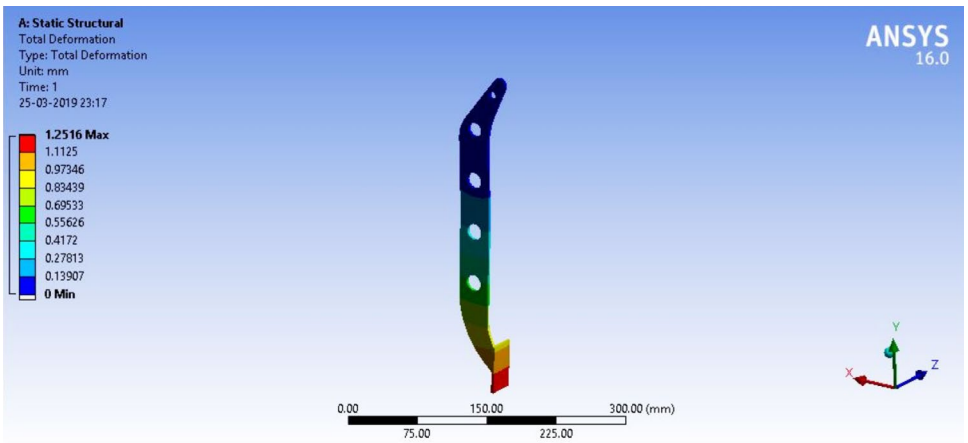

Fig. 6 Displacement of brake pedal

Tensile ultimate strength of material: 560 MPa
Tensile yield strength: 460 MPa
Factor of safety: 1.39
Maximum displacement: 2.177 mm.

Conclusions

An innovative, efficient lightweight braking system was designed, analysed and manufactured for an ATV. The

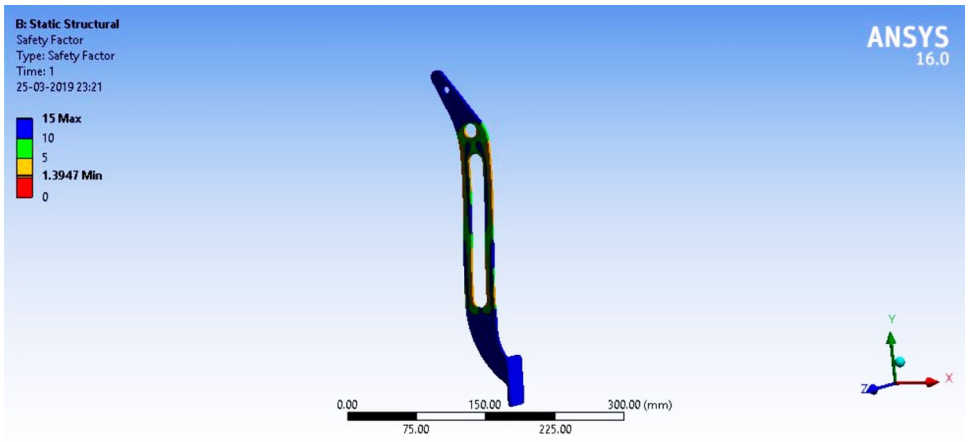

Fig. 7 FOS analysis of accelerator pedal

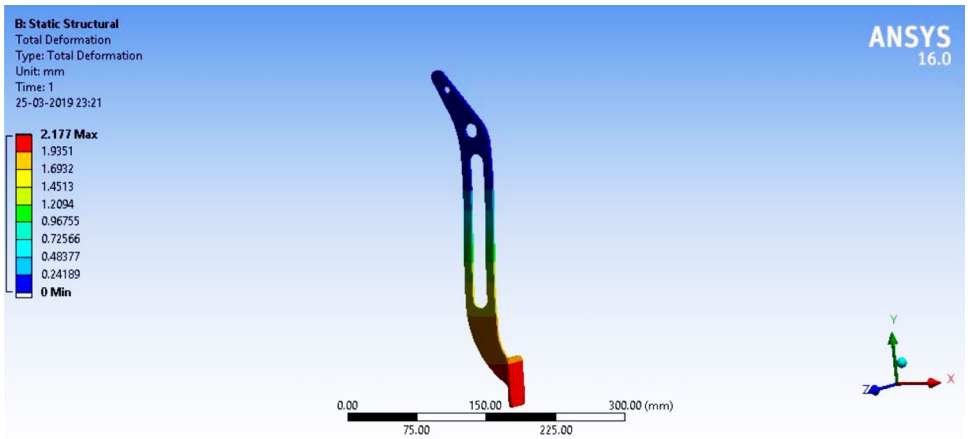

Fig. 8 Displacement of accelerator pedal

structural analysis and thermal analysis of the brake system showed that the designed brake discs are well within the safer limits for efficient working considering the respective factor of safety. The structural FOS obtained was 3.22 and the maximum temperature attained by the disc was 139 °C, and these values are within the acceptable limit for the considered design inputs. FOS and displacement analysis of the brake pedal shows that the design was satisfactory having a maximum displacement of 1.2516 mm for the considered loading and speed conditions. Analysis of the accelerator pedal with respect to FOS and having a maximum displacement of 2.177 mm shows the design was well within the considered norms and safe as per given load inputs. However, more research into materials can be done to increase the FOS of the parts. The cost of the disc brakes is higher when compared to the drum brakes. But, because the application was off-roading, safety was the top priority. Also, the braking distance obtained was 2.21 m. DOT4 braking fluid was used as a standard. The design weight and model could be optimized for better performance. The parts could be manufactured using metal materials, and material testing can be done to get actual practical values than ANSYS analysis.

Funding No funding or other financial assistance was given to this work.

Data availability Not applicable.

Declarations

Conflict of interest The writers claim that there aren't any conflicts of interest.

References

1. Polygon Engineering Date P3 & PC4, *Polygon Standard Design of Shafts and Hubs* (General Polygon Systems, Millville, 2001)
2. B. Ansell, The Brake Bible. 2008. November 2011 <http://www.pirate4x4.com/tech/billavista/Brakes/>
3. J. Shigley, J. Nisbett, R. Budynas, *Shigley's Mechanical Engineering Design* (McGraw-Hill, New York, 2011)
4. M.F. Ashby, *Material Selection in Mechanical Design*, 2nd edn. (Butterworth Heinemann, Oxford, 1999)
5. S.P. Jung, K.J. Jun, T.W. Park, J.H. Yoon, Development of the brake system design program for a vehicle. Int. J. Automot. Technol. **9**, 45–51 (2008)

6. S. Kulshreshtha, N. Varshney, S. Verma, S. Tiwari, R. Khanna, M. Kushwaha, Optimization in brake pedal of all-terrain vehicle. In *Advances in Engineering Design: Select Proceedings of FLAME 2020*. (Springer, Singapore, 2021), pp. 585–593
7. M. Mirajkar, P. Gurubaran, P. Jeevan Sunny, A. Konar, P.K. Ambadekar, Performance improvement of OEM brake caliper by manufacturing with design changes. In *Advances in Manufacturing Systems: Select Proceedings of RAM 2020* (Springer, Singapore, 2021), pp. 123–137
8. E. Hamilton, E. Klang, *Design of Formula SAE Brake Systems* (North Carolina State University, Raleigh, 2009)
9. N. Sergent, M. Tirovic, J. Voveris, Design optimization of an opposed piston brake caliper. Eng. Optim. **46**(11), 1520–1537 (2014)
10. A.T. Hamada, M.F. Orhan, An overview of regenerative braking systems. J. Energy Storage **52**, 105033 (2022)
11. N.A. Aziz, D.A. Wahab, R. Ramli, Establishment of engineering metrics for upgradable design of brake caliper. In *Sustainable Design and Manufacturing 2017: Selected papers on Sustainable Design and Manufacturing,* vol. 4 (Springer, 2017), pp. 87–97
12. A. Karamoozian, C.A. Tan, L. Wang, Squeal analysis of thin-walled lattice brake disc structure. Mater. Des. **149**, 1–14 (2018)
13. D. Wei, J. Song, Y. Nan, W. Zhu, Analysis of the stick-slip vibration of a new brake pad with double-layer structure in automobile brake system. Mech. Syst. Signal Process. **118**, 305–316 (2019)
14. N. Kudarauskas, Analysis of emergency braking of a vehicle. Transport **22**(3), 154–159 (2007)
15. A. Söderberg, S. Andersson, Simulation of wear and contact pressure distribution at the pad-to-rotor interface in a disc brake using general purpose finite element analysis software. Wear **267**(12), 2243–2251 (2009)
16. M. Poojari, H. Hanumanthappa, C. Durga Prasad, H.M. Jathanna et al., Computational modelling for the manufacturing of solar-powered multifunctional agricultural robot. Int. J. Interact. Des. Manuf. (2023). https://doi.org/10.1007/s12008-023-01291-y
17. M. Poojari, A. Raj, B.S. Babu, R. Muddaiah, B.S. Shreyas, Design, analysis of H-arm camber link rear suspension system along with design of custom coil springs for an electric all-terrain vehicle. Mater. Today Proc. **46**(7), 2858–2867 (2021)
18. M. Poojari, B.S. Shreyas, R. Muddaiah, A. Raj, B.S. Babu, Design, analysis of steering system and front suspension for an electric all-terrain vehicle. Mater. Today Proc. **46**(7), 2848–2857 (2021)
19. E. Denimal, J.J. Sinou, S. Nacivet, Influence of structural modifications of automotive brake systems for squeal events with kriging meta-modelling method. J. Sound Vib. **463**, 114938 (2019)
20. P. Mahajan, D. Gupta, V.K. Chawla, Design and analysis of brake disc assembly for an FSAE vehicle. Mater. Today Proc. **47**, 3407–3412 (2021)
21. M.H. Pranta, M.S. Rabbi, S.C. Banik, M.G. Hafez, Y.M. Chu, A computational study on structural and thermal behavior of modified disk brake rotors. Alex. Eng. J. **61**(3), 1882–1890 (2022)
22. M.T. Junior, S.N. Gerges, R. Jordan, Analysis of brake squeal noise using the finite element method: a parametric study. Appl. Acoust. **69**(2), 147–162 (2008)
23. C.B.N.S. Abhishikt, B. Ramachandran, G.N. Alekhya, Design and analysis of disk rotor brake under tribological behaviour of materials. Mater. Today Proc. **33**, 4298–4310 (2020)
24. T. Doyle, G. Wheatley, R.M. Nejad, N. Sina, Fatigue reliability assessment of the new design of universal upright for the JCU Formula SAE car. Structures **34**, 4113–4123 (2021)
25. V. Lakkannavar, K.B. Yogesha, C. Durga Prasad, M. Mruthunjaya, R. Suresh, A review on tribological and corrosion behavior of thermal spray coatings. J. Inst. Eng. (India) Ser. D (2024). https://doi.org/10.1007/s40033-024-00636-5
26. N. Praveen, U.S. Mallik, A.G. Shivasiddaramaiah, R. Hosalli, C. Durga Prasad, S. Bavan, Machinability study of Cu–Al–Mn shape memory alloys using Taguchi method. J. Inst. Eng. (India) Ser. D (2024). https://doi.org/10.1007/s40033-023-00629-w
27. N.G. Siddeshkumar, R. Suresh, C. Durga Prasad, L. Shivaram, N.H. Siddalingaswamy, Evolution of the surface quality and tool wear in the high speed turning of Al2219/n-B4C/MoS_2 metal matrix composites. Int. J. Cast Met. Res. (2023). https://doi.org/10.1080/13640461.2023.2285177
28. N. Praveen, U.S. Mallik, A.G. Shivasiddaramaiah, N. Nagabhushana, C. Durga Prasad, S. Kollur, Effect of CNC end milling parameters on Cu–Al–Mn ternary shape memory alloys using Taguchi method. J. Inst. Eng. (India) Ser. D (2023). https://doi.org/10.1007/s40033-023-00579-3
29. C. Durga Prasad, S. Kollur, C.R. Aprameya, T.V. Chandramouli, T. Jagadeesha, B.N. Prashanth, Investigations on tribological and microstructure characteristics of WC-12Co/FeNiCrMo composite coating by HVOF process. JOM J. Miner. Met. Mater. Soc. **1**, 1 (2023). https://doi.org/10.1007/s11837-023-06242-2
30. V. Srinivasa Chari, S. Jhavar, T.N. Sreenivasa, H. Hanumanthappa, C. Durga Prasad, B.K. Shanmugam, Impact of post-processing techniques on the wear resistance of plasma beam treatment on SS316L components. J. Inst. Eng. (India) Ser. D (2023). https://doi.org/10.1007/s40033-023-00584-6
31. S. Gotagunaki, V.S. Mudakappanavar, R. Suresh, C. Durga Prasad, Studies on the mechanical properties and wear behavior of an AZ91D magnesium metal matrix composite utilizing the stir casting method. Metallogr. Microstruct. Anal. (2023). https://doi.org/10.1007/s13632-023-01017-2
32. K.S. Lokesh, K. Shashank Kumar, N. Keerthan, R. Revanth, S. Sandeep, Sunil B. Lakkundi, V. Bharath, H. Hanumanthappa, C. Durga-Prasad, B.K. Shanmugam, Experimental analysis of the rice husk and eggshell powder-based natural fibre composite. J. Inst. Eng. (India) Ser. D. (2023). https://doi.org/10.1007/s40033-023-00557-9
33. G. Srinivasa-Rao, U. Mukkamala, H. Hanumanthappa, C. Durga Prasad, H. Vasudev, B. Shanmugam, K.C. Kishore Kumar, Evaluating and optimizing surface roughness using genetic algorithm and artificial neural networks during turning of AISI 52100 steel. Int. J. Interact. Des. Manuf. (2023). https://doi.org/10.1007/s12008-023-01549-5
34. C. Manjunatha, T.N. Sreenivasa, P. Sanjay, C. Durga Prasad, Optimization of friction stir welding parameters to enhance weld nugget hardness in AA6061-B_4C composite material. J. Inst. Eng. (India) Ser. D (2023). https://doi.org/10.1007/s40033-023-00562-y
35. C. Durga Prasad, S. Kollur, M. Nusrathulla, G. Satheesh Babu, M.B. Hanamantraygouda, B.N. Prashanth, N. Nagabhushana, Characterisation and wear behaviour of SiC reinforced FeNiCrMo composite coating by HVOF process. Trans. IMF (2023). https://doi.org/10.1080/00202967.2023.2246259
36. M. Arunadevi, M. Rani, R. Sibinraj, M.K. Chandru, C. Durga Prasad, Comparison of k-nearest neighbor & artificial neural network prediction in the mechanical properties of aluminum alloys. Mater. Today Proc. (2023). https://doi.org/10.1016/j.matpr.2023.09.111
37. H. Sharanabasava, M. Raviprakash, C. Durga Prasad, M.R. Ramesh, M.V. Phanibhushana, H. Vasudev, S. Kumar, Microstructure, mechanical and wear properties of SiC and Mo reinforced NiCr microwave cladding. Adv. Mater. Process. Technol. (2023). https://doi.org/10.1080/2374068X.2023.2257937
38. G.S. Kulkarni, N.G. Siddeshkumar, C. Durga Prasad, L. Shankar, R. Suresh, Drilling of GFRP with liquid silicon rubber reinforced with fine aluminium powder on hole surface quality and tool wear using DOE. J. Bio- Tribo-Corros. (2023). https://doi.org/10.1007/s40735-023-00771-8

39. S.D. Kulkarni, Manjunatha, U. Chandrasekhar, K.V. Manjunath, C. Durga Prasad, H. Vasudev, Design and optimization of polyvinyl-nitride rubber for tensile strength analysis. Int. J. Interact. Des. Manuf. (2023). https://doi.org/10.1007/s12008-023-01405-6
40. N. Praveen, U.S. Mallik, A.G. Shivasiddaramaih, R. Suresh, C. Durga Prasad, L. Shivaramu, Synthesis and wire EDM characteristics of Cu–Al–Mn ternary shape memory alloys using Taguchi method. J. Inst. Eng. India Ser. D (2023). https://doi.org/10.1007/s40033-023-00501-x
41. C. Durga Prasad, S. Joladarashi, M.R. Ramesh, M.S. Srinath, B.H. Channabasappa, Effect of microwave heating on microstructure and elevated temperature adhesive wear behavior of HVOF deposited CoMoCrSi–Cr_3C_2 composite coating. Surf. Coat. Technol. **374**, 291–304 (2019). https://doi.org/10.1016/j.surfcoat.2019.05.056
42. G. Madhu Sudana Reddy, C. Durga Prasad, S. Kollur, A. Lakshmikanthan, R. Suresh, C.R. Aprameya, Investigation of high temperature erosion behaviour of NiCrAlY/TiO_2 plasma coatings on titanium substrate. JOM J. Miner. Met. Mater. Soc. (2023). https://doi.org/10.1007/s11837-023-05894-4
43. N. Praveen, U.S. Mallik, A.G. Shivasiddaramaih, R. Suresh, L. Shivaramu, C. Durga Prasad, M. Gupta, Design and analysis of shape memory alloys using optimization techniques. Adv. Mater. Process. Technol. (2023). https://doi.org/10.1080/2374068X.2023.2208021
44. C. Durga Prasad, A. Jerri, M.R. Ramesh, Characterization and sliding wear behavior of iron based metallic coating deposited by HVOF process on low carbon steel substrate. J. Bio Tribo-Corros. **6**, 69 (2020). https://doi.org/10.1007/s40735-020-00366-7
45. G. Madhusudana Reddy, C. Durga Prasad, P. Patil, N. Kakur, M.R. Ramesh, High temperature erosion performance of NiCrAlY/Cr_2O_3/YSZ plasma spray coatings. Trans. IMF (2023). https://doi.org/10.1080/00202967.2023.2208899
46. C. Durga-Prasad, S. Joladarashi, M.R. Ramesh, M.S. Srinath, B.H. Channabasappa, Comparison of high temperature wear behavior of microwave assisted HVOF sprayed CoMoCrSi-WC-CrC-Ni/WC-12Co composite coatings. Silicon **12**, 3027–3045 (2020). https://doi.org/10.1007/s12633-020-00398-1
47. H. Sharanabasva, C. Durga Prasad, M.R. Ramesh, Characterization and wear behavior of NiCrMoSi microwave cladding. J Mater Eng Perform (2023). https://doi.org/10.1007/s11665-023-07998-zc
48. C. Durga-Prasad, S. Joladarashi, M.R. Ramesh, M.S. Srinath, B.H. Channabasappa, Microstructure and Tribological Behavior of Flame Sprayed and Microwave Fused CoMoCrSi/CoMoCrSi-Cr_3C_2 Coatings. Mater. Res. Express **6**, 026512 (2019). https://doi.org/10.1088/2053-1591/aaebd9
49. G. Madhusudana Reddy, C. Durga Prasad, P. Patil, N. Kakur, M.R. Ramesh, Investigation of plasma sprayed NiCrAlY/Cr_2O_3/YSZ coatings on erosion performance of MDN 420 steel substrate at elevated temperatures. Int. J. Surf. Sci. Eng. **17**(3), 180–194 (2023). https://doi.org/10.1504/IJSURFSE.2023.10054266
50. H. Sharanabasva, C. Durga Prasad, M.R. Ramesh, Effect of Mo and SiC reinforced NiCr microwave cladding on microstructure, mechanical and wear properties. J. Inst. Eng. India Ser. D (2023). https://doi.org/10.1007/s40033-022-00445-8
51. C. Durga Prasad, S. Joladarashi, M.R. Ramesh, M.S. Srinath, B.H. Channabasappa, Development and sliding wear behavior of Co–Mo–Cr–Si cladding through microwave heating. Silicon **11**, 2975–2986 (2019). https://doi.org/10.1007/s12633-019-0084-5
52. H.S. Nithin, K.M. Nishchitha, D.G. Pradeep, C. Durga Prasad, M. Mathapati, Comparative analysis of CoCrAlY coatings at high temperature oxidation behavior using different reinforcement composition profiles. Weld. World **67**, 585–592 (2023). https://doi.org/10.1007/s40194-022-01405-2
53. V. Gowda, H. Hanumanthappa, B.K. Shanmugam, C. Durga Prasad, T.N. Sreenivasa, M.S. Rajendra Kumar, High-temperature tribological studies on hot forged Al6061-Tib_2 in-situ composites. J. Bio Tribo-Corros. **8**, 101 (2022). https://doi.org/10.1007/s40735-022-00699-5
54. G. Madhusudana Reddy, C. Durga Prasad, G. Shetty, M.R. Ramesh, T. Nageswara Rao, P. Patil, Investigation of thermally sprayed NiCrAlY/TiO_2 and NiCrAlY/Cr_2O_3/YSZ cermet composite coatings on titanium alloys. Eng. Res. Express **4**, 025049 (2022). https://doi.org/10.1088/2631-8695/ac7946
55. G. Madhusudana Reddy, C. Durga Prasad, P. Patil, N. Kakur, M.R. Ramesh, Elevated temperature erosion performance of plasma sprayed NiCrAlY/TiO_2 Coating on MDN 420 steel substrate. Surf. Topogr. Metrol. Prop. **10**, 025010 (2022). https://doi.org/10.1088/2051-672X/ac6a6e
56. T. Naik, M. Mathapathi, C. Durga Prasad, H.S. Nithin, M.R. Ramesh, Effect of laser post treatment on microstructural and sliding wear behavior of HVOF sprayed NiCrC and NiCrSi coatings. Surf. Rev. Lett. **29**(1), 225000 (2022). https://doi.org/10.1142/S0218625X2250007X
57. M. Mathapati, K. Amate, C. Durga Prasad, M.L. Jayavardhana, T. Hemanth Raju, A review on fly ash utilization. Mater. Today Proc. **50**(5), 1535–1540 (2022). https://doi.org/10.1016/j.matpr.2021.09.106
58. G. Madhusudana Reddy, C. Durga Prasad, G. Shetty, M.R. Ramesh, T. Nageswara Rao, P. Patil, High temperature oxidation behavior of plasma sprayed NiCrAlY/TiO_2 & NiCrAlY/Cr_2O_3/YSZ coatings on titanium alloy. Weld World (2022). https://doi.org/10.1007/s40194-022-01268-7
59. G. Madhusudana Reddy, C. Durga Prasad, G. Shetty, M.R. Ramesh, T. Nageswara Rao, P. Patil, High temperature oxidation studies of plasma sprayed NiCrAlY/TiO_2 & NiCrAlY/Cr_2O_3/YSZ cermet composite coatings on MDN-420 special steel alloy. Metallogr. Microstruct. Anal. **10**, 642–651 (2021). https://doi.org/10.1007/s13632-021-00784-0
60. R. Dinesh, S. Rohan Raykar, T.L. Rakesh, M.G. Prajwal, M. Shashank Lingappa, C. Durga Prasad, Feasibility study on MoCoCrSi/ WC-Co cladding developed on austenitic stainless steel using microwave hybrid heating. J. Mines Met. Fuels (2021). https://doi.org/10.18311/jmmf/2021/30113
61. C. Durga Prasad, S. Lingappa, S. Joladarashi, M.R. Ramesh, B. Sachin, Characterization and sliding wear behavior of CoMoCrSi + Flyash composite cladding processed by microwave irradiation. Mater. Today Proc. **46**, 2387–2391 (2021). https://doi.org/10.1016/j.matpr.2021.01.156
62. G. Madhu, K.M. Mrityunjaya Swamy, D. Ajay Kumar, C. Durga Prasad, U. Harish, Evaluation of hot corrosion behavior of HVOF thermally sprayed Cr_3C_2–35NiCr coating on SS 304 boiler tube steel. Am. Inst. Phys. **2316**, 030014 (2021). https://doi.org/10.1063/5.0038279
63. M. Reddy, C.D. Prasad, P. Patil, M.R. Ramesh, N. Rao, Hot corrosion behavior of plasma sprayed NiCrAlY/TiO_2 and NiCrAlY/Cr_2O_3/YSZ cermets coatings on alloy steel. Surf. Interfaces **22**, 100810 (2021). https://doi.org/10.1016/j.surfin.2020.100810
64. C. Durga Prasad, S. Joladarashi, M.R. Ramesh, M.S. Srinath, Microstructure and tribological resistance of flame sprayed CoMoCrSi/WC-CrC–Ni and CoMoCrSi/WC–12Co composite coatings remelted by microwave hybrid heating. J. Bio Tribo-Corros. **6**, 124 (2020). https://doi.org/10.1007/s40735-020-00421-3
65. K.G. Girisha, K.V. Sreenivas Rao, C. Durga Prasad, Slurry erosion resistance of martenistic stainless steel with plasma sprayed Al_2O_3–40%TiO_2 coatings. Mater. Today Proc. **5**, 7388–7393 (2018). https://doi.org/10.1016/j.matpr.2017.11.409
66. C. Durga Prasad, S. Joladarashi, M.R. Ramesh, Comparative investigation of HVOF and flame sprayed CoMoCrSi coating.

Am. Inst. Phys. **2247**, 050004 (2020). https://doi.org/10.1063/5.0003883
67. C. Durga Prasad, S. Joladarashi, M.R. Ramesh, M.S. Srinath, B.H. Channabasappa, Influence of microwave hybrid heating on the sliding wear behaviour of HVOF sprayed CoMoCrSi coating. Mater. Res. Express **5**, 086519 (2018). https://doi.org/10.1088/2053-1591/aad44e
68. K.G. Girisha, C. Durga Prasad, K.C. Anil, K.V. Sreenivas Rao, Dry sliding wear behaviour of Al2O3 coatings for AISI 410 grade stainless steel. Appl. Mech. Mater. **766–767**, 585–589 (2015). https://doi.org/10.4028/www.scientific.net/AMM.766-767.585
69. C. Durga-Prasad, S. Joladarashi, M.R. Ramesh, A. Sarkar, High temperature gradient cobalt based clad developed using microwave hybrid heating. Am. Inst. Phys. **1943**, 020111 (2018). https://doi.org/10.1063/1.5029687
70. K.G. Girisha, R. Rakesh, C. Durga Prasad, K.V. Sreenivas Rao, Development of corrosion resistance coating for AISI 410 grade steel. Appl. Mech. Mater. **813–814**, 135–139 (2015). https://doi.org/10.4028/www.scientific.net/AMM.813-814.135